Development of a Mobile Tomographic Gamma Camera Based on Ectomography

Cardiotom

by

Mikael Persson

Department of Medical Laboratory Sciences and Technology, Division of Medical Engineering, Karolinska Institutet, S-14181 Huddinge, Sweden

Stockholm 2001

THIS PAGE IS INTENTIONALLY LEFT BLANK

This thesis is based on the following peer reviewed publications and conference records, which will be referred to by the roman numerals I - IX

Peer reviewed publications

I. Dale S, Holmberg M, Larsson H, Persson M, Ribbe T, Elmqvist H, Bone D, Brodin L-Å, Lindström C, Jorfeldt L. A mobile tomographic gamma camera system for acute studies.

IEEE Trans Nucl Sci 1997; 44:199-203.

II. M. Persson, S. Dale. Effects of Non-Optimal Acquisition Geometry in Myocardial Perfusion Imaging Using Ectomography.

IEEE Trans Nucl Sci 1998; 6: 3142-3148.

III. Bone D, Dale S, Segawa, D, Wang Q-D, Gonon A, Persson M, Rydén L. A mobile tomographic gamma camera system for quantification of myocardial perfusion: an experimental study.

Submitted J. Nucl. Card.

IV. Persson M, Bone D, Elmqvist H. Total Variation Norm for 3-Dimensional Iterative Reconstruction in Limited View Angle Tomography.

Phys. Med Biol. 2001;46: 853-866.

V. Persson M, Bone D, Elmqvist H. 3-Dimensional Total Variation Norm for SPECT reconstruction.

Nucl. Instr. Meth. Phys. Res. A. In print.

VI. Bone D, Persson M, Ribbe T, Dale S. Beside tomographic scintigraphy: a diagnostic tool in intensive care and the emergency room

Nucl. Instr. Meth. Phys. Res. A. In print.

Conference records

VII. Persson M, Schaumann T, Dale S, Bone D, Lindström C. Suppression of Artifacts Due to Data Truncation When Using Segmented Slant Hole Collimators in Ectomography.

IEEE Medical Imaging Conference 1998. Conf. Rec. ISBN 0-7803-5024-3.

VIII. Lyckman C, Dale S, Persson M, Bone D. Cerebral blood flow imaging using Ectomography – a feasablilty study.

IEEE Medical Imaging Conference 1998. Conf. Rec. ISBN 0-7803-5024-3

IX. Persson M, Bone D, Meissinger K. Resolution recovery in Ectomography using filtered backprojection.

IEEE Medical Imaging Conference 1998. Conf. Rec. ISBN 0-7803-5699-3

THIS PAGE IS INTENTIONALLY LEFT BLANK

Contents

Glossary

Planar image	Two-dimensional representation of three dimensional object
Section	Slice through an object with a defined thickness.
Section image	Reconstructed image of a section
Projection	A planar image used to reconstruct section images. See tomography.
View angle	The angel between the direction of projection and the axis of rotation of the detector.
Limited view angle tomography *or* Restricted view angle tomography	Tomographic imaging with a view angle of less than 90°.
Ectomography	Tomography with a limited view angle and many projections.
CT	Computed Tomography
Cardiotom	A mobile tomographic gamma camera based on Ectomography, using a rotating slant hole collimator to achieve varying projection direction.
ER	Emergency room
ICU	Intensive care unit
PET	Positron Emission Tomography
MRI	Magnetic Resonance Imaging.
fMRI	Functional Magnetic Resonance Imaging.
SPECT	Single Photon Emission Computed Tomography. Same as SPET
SPET	Single Photon Emission Tomography. Same as SPECT.
Pixel	Abbreviation of picture element
Voxel	Abbreviation of volume element

α	Slant angle of a slant hole collimator, equivalent to the view angle in a tomographic system using a rotating slant hole collimator, such as Cardiotom.
θ	Projection direction, determined by the detector position in SPECT or collimator rotation in the Cardiotom system.
$\delta(x)$	The Dirac function.
$P(\theta,t)$	The projection at detector rotation θ along the detector position t.
$f(x,y)$	Representation of a two-dimensional object in Cartesian coordinates.
$f(x,y,z)$	Representation of a three-dimensional object in Cartesian coordinates.
$F(u,v)$	Representation of a two-dimensional object in Fourier space.
$F(u,v,w)$	Representation of a three-dimensional object in Fourier space.

Introduction

Medical imaging is today an important clinical tool in the diagnosis of many diseases and in research. Medical imaging can be divided into two categories; anatomical and functional imaging. Anatomical imaging is concerned with the structure and composition of tissues, such as imaging of bone fractures using x-rays. Functional imaging on the other hand, aims at extracting information regarding the physiological function of organs, such as the distribution of glucose metabolism in the brain.

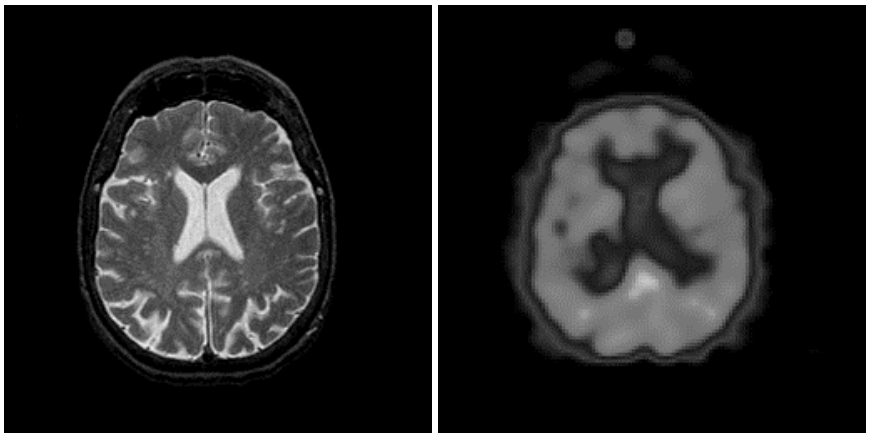

Figure 1. Study of a normal brain: anatomical image from an MRI study (left) and functional image from a SPECT study (right) showing blood perfusion.

Figure 1 illustrates the difference between functional imaging and anatomical imaging of the brain. The anatomical image is from a study using magnetic resonance imaging (MRI), and the functional image is from a Single Photon Emission Computed Tomography (SPECT) study. The SPECT image in this particular case shows blood perfusion in the brain.

When we discuss images, we usually think of them as being two-dimensional (2D), however, since our environment is inherently three-dimensional (3D), it is in many cases advantageous, or even necessary, to perform 3D imaging. In 3D imaging, the primary acquired data are still two-dimensional. However, the theory of tomography supplies the necessary tools for 3D image reconstruction.

In tomography, the acquired images are called projections, since each image represents a projection of a 3D object onto a 2D image. The Fourier slice theorem states that we have enough information to accurately reconstruct a 3D object from the projections if a large number of projection images are acquired with different orientation. It is then possible to extract 2D images of arbitrary orientation from the reconstructed 3D data, present them on a screen or make a hardcopy, and perform accurate measurements in these images. A comparison between planar and tomographic images is shown in Figure 2.

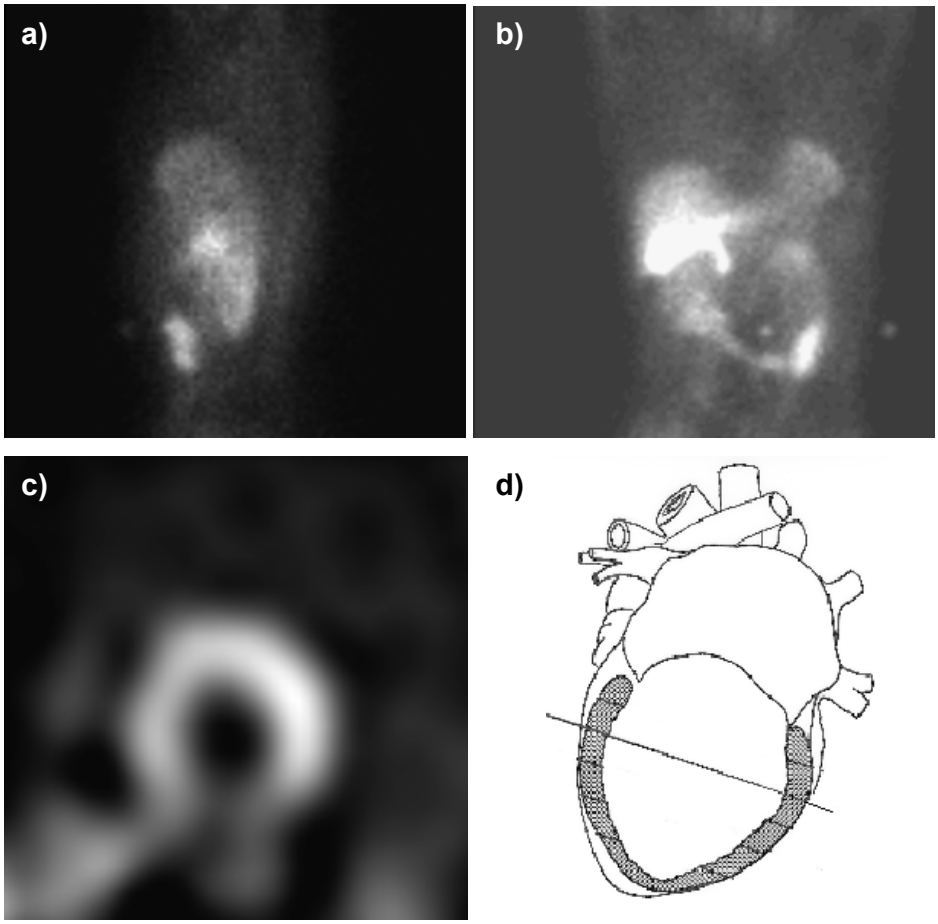

Figure 2. The difference between planar and tomographic images from a heart stress study using 99mTc SPECT. a) a planar frontal view, b) is a planar lateral view, c) a short axis slice from a tomographic reconstruction, d) the approximate orientation of the short axis slice.

Overview of modalities

The most common medical imaging technique today is probably diagnostic x-ray imaging, where the result of the procedure is a 2D anatomical image. In x-ray imaging the patient is irradiated with x-ray photons and the amount of x-rays transmitted through the patient is recorded on a film or a detector. This is known as a transmission image and is a measure of x-ray attenuation. While this may provide sufficient information in many cases, for instance, when dealing with bone fractures, there is often a need to determine localization and extent in 3 dimensions.

Computed Tomography (CT) is a tomographic imaging method, and as the information given in the projection data is the attenuation of x-ray through an object, the reconstruction will show the attenuation coefficients of the matter, or tissue in the case of a patient. The attenuation is dependent on the (electron) density of the tissue, and allows the anatomy of the body to be imaged.

Functional imaging, on the other hand, aims at determining the function of an organ, for instance glucose metabolism in the brain, or blood perfusion in the myocardium. Functional imaging can be performed with nuclear medicine or functional magnetic resonance imaging (fMRI).

In nuclear medicine, a chemical substance, which is part of the metabolism of the organ of interest, is labelled with a radioactive isotope. This compound, or tracer, is then injected into the patient, transported though the blood and taken up in the organ as part of the metabolic process. Since the commonly used isotopes decay through the emission of gamma photons, the amount of tracer taken up can then be measured by counting the gamma-photons emitted. Commonly used isotopes include ^{99m}Tc, ^{201}Tl and ^{131}I and ^{123}I, which are single photon emitters.

Other substances used are ^{15}O, ^{13}N, and ^{11}C, which are positron emitters used in Positron Emission Tomography (PET).

Positron imaging

An emitted positron will travel a short distance, usually <5mm, and undergo an annihilation process, in which photons are produced.

In most cases, two annihilation photons are created, with an energy of 511 keV each travelling in ~180° opposing directions. There are cases when three or more photons are created, however this is relatively rare, and the since the sum of the photon energies equals the positron resting mass (1.02 MeV), such photons will each have an energy lower than 511 keV. The PET detector consists of a ring of detector elements. When two 511 keV photons are detected in coincidence by two detector elements, the emission can be localized along a straight line between these two detectors. Acquisition data is stored as sinograms, which are the projection data. Tomographic image reconstruction techniques are used to reconstruct images from the acquired data.

Gamma camera imaging

In radionuclide imaging, the most common system is an instrument called the gamma camera. Radionuclide imaging with a gamma camera is also called scintigraphy. The gamma camera is sometimes referred to as Anger camera, after the inventor Hal O. Anger. The principle of the gamma camera [1] was described by Anger in 1958 based on analogue circuitry. Modern gamma cameras employ digital circuitry to an increasing extent, but the underlying principle is still similar to the concept of Anger.

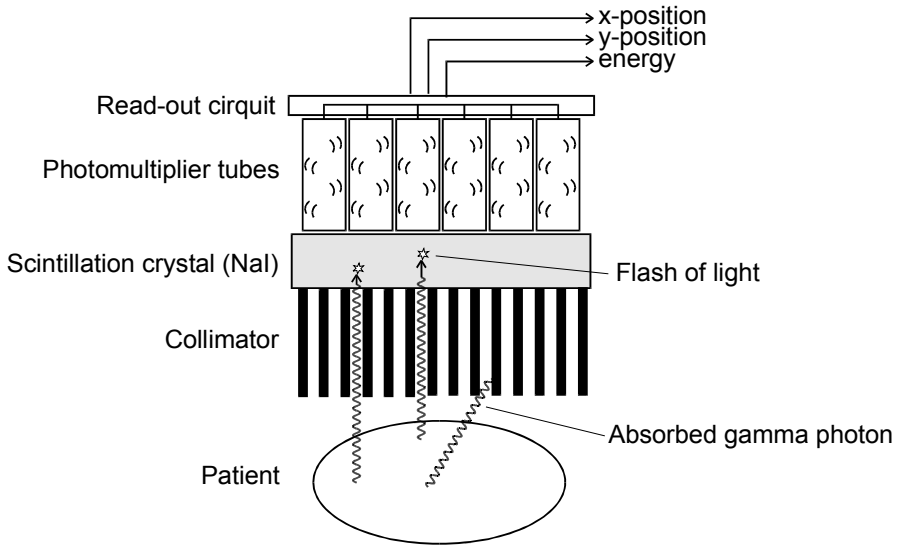

Figure 3. Schematic view of a gamma camera.

The principal components of the gamma camera are the collimator, scintillation crystal, photomultiplier tubes and the read-out circuitry, as shown in figure 3. As the radionuclide administered to the patient decays, γ-photons are emitted. The collimator consists of a dense material, usually lead, with parallel holes that are most often hexagonal in shape. Photons travelling in a direction approximately parallel to the holes will reach the scintillation crystal, other photons will be absorbed by the lead in the septa. The scintillation crystal is usually made of sodium iodide (NaI) doped with thallium (Tl). When γ-photons are absorbed, the energy is converted to a flash of visible light. The intensity of the light is proportional to the energy of the absorbed γ-photon. Light is collected by the photomultiplier tubes, light photons are converted to electrons and the signal is then amplified before being processed by the read-out circuit. The read-out circuit calculates the x- and y-position of the scintillation, as well as supplying a signal proportional to the energy of the γ-photon, that caused the scintillation.

The gamma camera is used in both planar (2-dimensional) imaging and tomographic imaging. Tomographic imaging is called Single Photo Emission Computed Tomography and most often referred to by the acronym, SPECT or SPET.

Planar scintigraphy is often used for lung perfusion, dynamic studies and in whole body scans in diagnosis of skeletal cancer, whereas tomography is used for heart and brain scintigraphy. More specifically, SPECT is often used for cardiac perfusion studies as a part of the diagnosis of myocardial infarction, and also in diagnosis of diseases of the brain, such as dementia or cancer.

In SPECT, projection images are collected one at a time by stepwise rotating the detector, around the patient. Usually 64 to 128 projections are collected over a detector rotation of 180° or 360°. Since the detector has to be shielded from external radiation, the detector head is very heavy, and requires a robust and massive gantry, which is floor mounted.

To increase system sensitivity modern SPECT systems are often equipped with two or three detector heads. This increase in sensitivity can be utilized either to reduce radiation dose to the patient and/or scan times, or to improve image statistics i.e. reduce noise levels in projection images.

In gamma camera imaging, the directions of incident photons are determined by mechanical collimation. Compared to the electronic coincidence collimation used in PET, the mechanical collimation limits the system sensitivity, since more than 99% of the photons arriving at the collimator are absorbed in the lead.

Despite the superior sensitivity of PET, SPECT is more widely used clinically. There are a number of reasons for this. For instance, the isotopes used for SPECT imaging have a half life of at least 6 hours and compounds can be prepared within the department, while the majority of PET isotopes have short half-lives (< 20 minutes), and must be produced in a cyclotron near the imaging equipment. This requirement and the fact that the PET machine is more complex, makes PET imaging much more expensive than SPECT and PET systems are uncommon, even though they are superior to SPECT systems in providing quantitative information.

A recent development has been to modify dual headed SPECT systems to enable coincidence imaging, making positron and single photon imaging possible with a single system. However, sensitivity in coincidence mode is considerably lower than for a dedicated PET system, since the detector of the SPECT system are two planar cameras (detectors), whereas a dedicated PET system has a ring of detectors surrounding the patient, hence, a large fraction of photons will be lost in a coincidence SPECT system compared to a PET system.

Cardiotom – clinical applications

SPECT is often used in the diagnosis of myocardial infarction. Patients suffering from suspected acute myocardial infarction arrive at the emergency room (ER) with chest pain. However, the presence of chest pain can be caused by other conditions. It has been shown in studies that failure to correctly identify the cause of chest pain at the time of admission can be reduced by performing myocardial scintigraphy in the ER [2,3,4]. In this situation it would be beneficial to have a mobile unit that can perform tomographic scintigraphy readily available in the ER.

Scintigraphic imaging with SPECT can also be of value in the Intensive Care Unit where patients are connected to monitoring and life support equipment, or even in the Operating Theatre.

Most currently available tomographic imaging systems are large and stationary installations to which the patient must be transported. There are some mobile gamma cameras available commercially, but to my knowledge none of these have tomographic capabilities. Due to the need to transport patients to the gamma camera system, scintigraphic imaging is not generally performed on seriously ill patients, even when the diagnostic information obtained could be of great value in patient management

The Cardiotom system is a tomographic gamma camera system, based on a commercially available detector system. Tomographic imaging is achieved by rotating a collimator with parallel and slanted holes in front of the stationary detector. The method of acquisition is a form of limited view angle tomography called Ectomography [5]. Since only the collimator is rotated during the acquisition of data, the camera gantry is relatively simple, and the technique can be implemented on a mobile gamma camera system.

As mentioned earlier, SPECT is often used in the diagnosis of myocardial infarction. Patients suffering from suspected acute myocardial infarction arrive at the emergency room (ER) with chest pain. However, the presence of chest pain can be caused by other conditions. It has been shown in studies in the USA that failure to correctly identify the cause of chest pain at the time of admission can be reduced by performing myocardial scintigraphy in the ER [6,7,8]. In this situation it would be beneficial to have a mobile unit that can perform tomographic scintigraphy readily available in the ER.

Other applications for a mobile system, such as Cardiotom, can be in the intensive care unit where patients are connected to monitoring and life support equipment, or in cases where the patient is too ill to be transported to a stationary SPECT system. Another possible application is in the operating room for intra-operative imaging.

Aims of the study

- To develop software and hardware for a mobile tomographic gamma camera system: the Cardiotom
- To evaluate the limitations of Ectomography when using filtered back projection for reconstruction
- To develop a method of reconstruction that compensates for the incomplete data acquisition with Ectomography
- To demonstrate that a mobile tomographic system can be used in a clinical situation

Materials and methods

Acquisition geometry

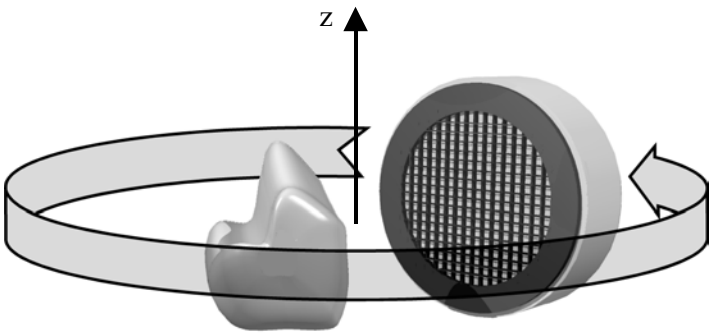

Figure 4. The acquisition geometry of a traditional SPECT system. The axis of rotation is z*.*

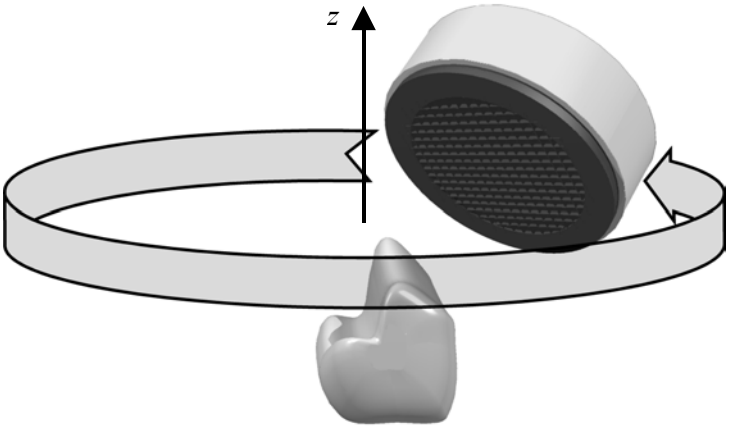

Figure 5. One possible acquisition geometry for Ectomography. The axis of rotation is z*.*

Consider a gamma camera equipped with a parallel hole collimator. Figure 4 then shows the acquisition geometry of a SPECT system, where the normal of the detector surface is perpendicular to the axis of rotation. In Ectomography the angle between the axis of rotation and the normal of the detector surface is less than 90°, as shown in figure 5. In both cases, the whole camera detector must be moved to obtain different projection directions.

If, however, the gamma camera is equipped with a collimator with slanted, parallel holes, different projection directions can be obtained by rotating the collimator in front of a stationary detector, as shown in figure 6.

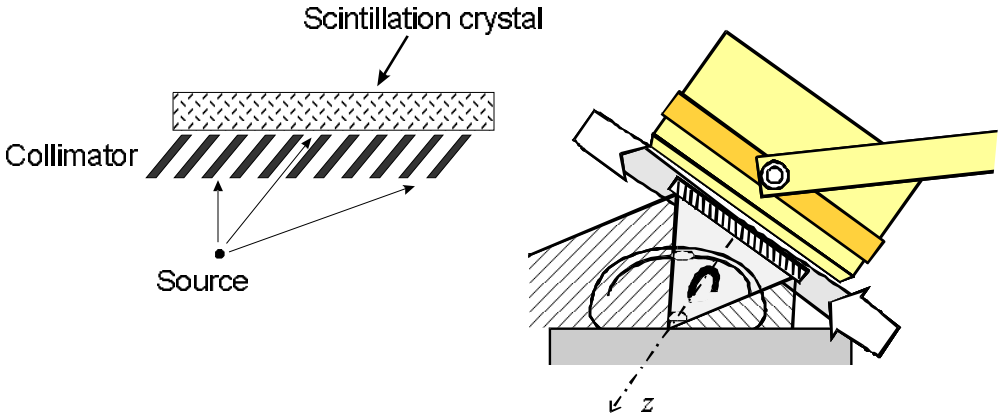

Figure 6. The acquisition geometry of Ectomography using a rotating slant hole collimator.

The volume covered in all projection images will constitute a cone with the base at the collimator. This is called the common reconstruction volume. As seen in figure 6, there is also a larger volume which will be only partially covered, i.e. not present in all projection images. The *z*-direction has been defined as perpendicular to the detector surface (i.e. along the axis of rotation), and z increases with distance from the detector.

The Fourier slice theorem

The basis for tomographic imaging could be said to be the Radon transform. It was formulated by Johann Radon in 1917 [9], and is the mathematical formulation of the projection data acquisition. Assuming we have an object which can be described by a 2D-function $f(x,y)$, the Radon transform can be written as

$$P(\theta,t) = \mathbf{R}f(x,y) = \int_{-\infty}^{\infty}\int_{-\infty}^{\infty} f(x,y)\delta(x\cos\theta + y\sin\theta - t)dxdy \qquad (1)$$

$P(\theta, t)$ is the projection at detector rotation θ along the detector position t. This relationship can be interpreted as a 1D projection being defined by a set of parallel line integrals through a 2D object. Each point in the Radon space is defined as one line integral through the 2D object.

The 2D Fourier slice theorem describes the mathematical relationship between the 2D object and the 1D projection in the Fourier domain or, put in another way, the relationship between the Radon transform and the object in the Fourier domain.

The 2D Fourier slice theorem can be formulated in the following way: The Fourier transform of a 1D projection at angle θ, $P(\theta, t)$, t: $-\infty \rightarrow -\infty$,yields data identical to those found along a line with the same orientation θ through the 2D Fourier transform of the object.

There is a corresponding relationship dealing with 3D object projected onto a 2D projection, called the Central slice theorem. This is a variant of the 3D Fourier slice theorem, formulated as follows: suppose we have a 2D parallel projection of a 3D object, where the normal of the projection is parallel to the projection direction**.** The 2D Fourier transform of the projection will then correspond to a central slice through the 3D Fourier transform of the object, with a normal parallel to the projection direction. This is illustrated in figure 7.

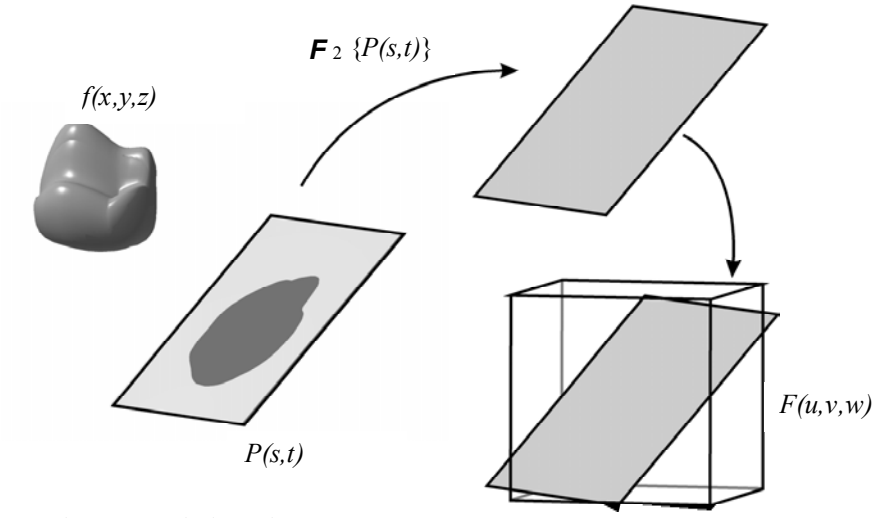

Figure 7. The Central slice theorem.

Assuming that the signal is band-limited in some sense, regular tomography with an infinite number of projections would fill a sphere in the Fourier domain. Figure 8 shows how 4 projections over a rotation of 180° would be mapped into Fourier space. In this case the angle between the detector and axis of rotation is 90°, which is the situation in for instance SPECT.

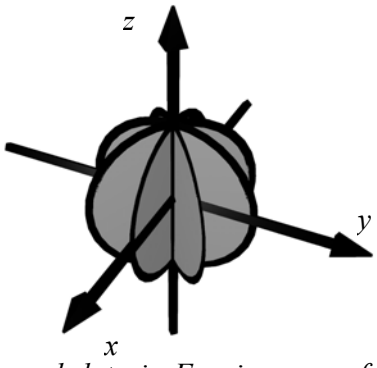

Figure 8. An example of measured data in Fourier space from 4 projections using SPECT geometry.

In Ectomography, the angle between the detector surface and axis of rotation is less than 90°, and the projections acquired will correspond to planes in the Fourier space not parallel to the axis of rotation, *z*. Tomography with this type of geometry is also known as restricted view angle tomography or limited view angle tomography. As projection images are acquired from different projection directions, a partial sphere will be filled with data in Fourier space. There will be volumes in the Fourier space not covered by any projection direction as the projection plane is tilted with respect to the axis of rotation. As the number of projections increases, the shape of the empty volume will approach a cone, hence it is called the empty cone.

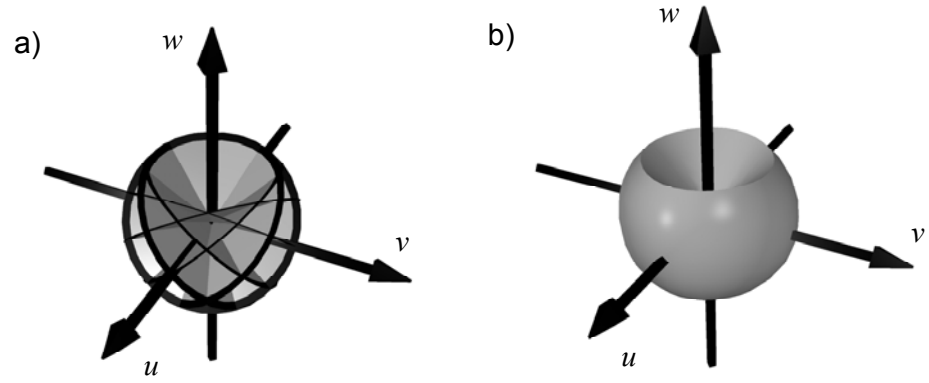

Figure 9. The origin of the empty cone in the Fourier domain using restricted view angle tomography, a) showing the result after 8 projections acquired over 360° detector rotation and b) shows the how data is mapped when the number of projection is large.

The missing data phenomenon is a property common to all limited view angle methods, and will cause some artefacts in the reconstructed volume. Since data is missing along the *z*-axis, which is the depth direction in an Ectomographic system, the result is limited depth resolution. The volume of the empty cone is dependent on the view angle that in the Cardiotom system translates into the collimator slant angle. A greater slant angle makes the volume of the empty cone smaller, hence improving depth resolution, and reducing artefacts stemming from the empty one. However, the trade off is a reduction of the volume in which the imaged object can be fully reconstructed, as shown in figure 10.

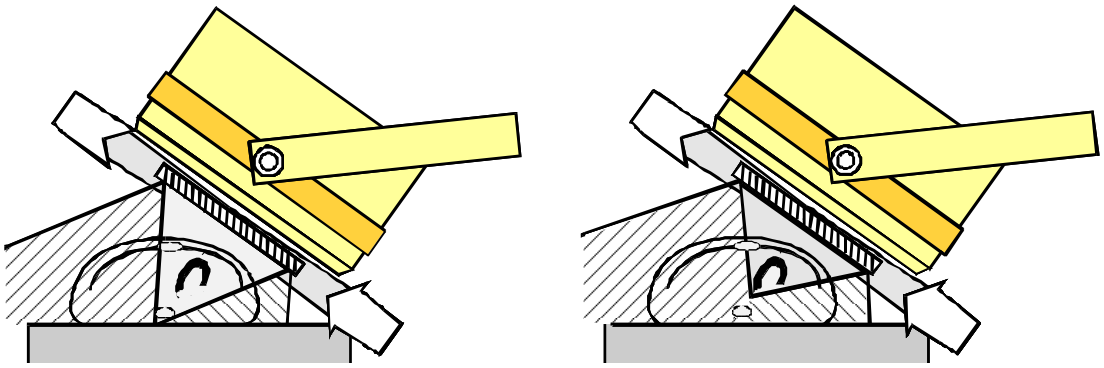

Figure 10. A smaller slant angle (left) yields a larger empty cone, but also a larger volume, which can be fully reconstructed, compared to a larger slant angle (right), with a smaller empty cone resulting in better depth resolution.

Image reconstruction

Filtered back-projection

In order to perform the inverse Radon transform, the Fourier slice theorem states that the sample density of low frequency components must be elevated in comparison to the high frequency components. The result is that the projection images should be subjected to a high-pass filtration before they are back projected into the reconstruction volume; hence the name filtered back-projection (FBP).

The filtered back-projection can be derived by applying the Fourier slice theorem and the inverse Fourier transform. Assuming that the 2D Fourier transform $F(u,v)$ of the object function $f(x,u)$ is known, the inversion of $F(u,v)$ can be expressed as:

$$f(x,y) = \int_{-\infty}^{\infty}\int_{-\infty}^{\infty} F(u,v)\exp(j2\pi(ux+vy))dudv \qquad (2)$$

Replacing the Cartesian coordinate system by polar coordinates requires the following substitutions:

$$\begin{aligned} u &= r\cos\phi \\ v &= r\sin\phi \\ dudv &= rd\phi dr \end{aligned} \qquad (3)$$

The inverse Fourier representation of the object can then be written as:

$$\begin{aligned} f(x,y) &= \int_{0}^{2\pi}\int_{0}^{\infty} F(r,\phi)r\exp(j2\pi r(x\cos\phi + y\sin\phi))drd\phi \\ &= \int_{0}^{\pi}\int_{0}^{\infty} F(r,\phi)r\exp(j2\pi r(x\cos\phi + y\sin\phi))drd\phi \\ &+ \int_{\pi}^{2\pi}\int_{0}^{\infty} F(r,\phi)r\exp(j2\pi r(x\cos\phi + y\sin\phi))drd\phi \end{aligned} \qquad (4)$$

Using the following observation

$$F(r,\phi+\pi) = F(-r,\phi) \qquad (5)$$

the inverse Fourier transform can be written as:

$$f(x,y) = \int_{0}^{\pi}\int_{-\infty}^{\infty} F(r,\phi)|r|\exp(j2\pi r(x\cos\phi + y\sin\phi))drd\phi \qquad (6)$$

By considering the Fourier slice theorem, the 2 D Fourier transform of the object along lines through the origin can be replaced by the 1 D Fourier transform of the projection data $S_\phi(r)$:

$$f(x,y) = \int_{0}^{\pi}\left[\int_{0}^{\infty} S_\phi(r)|r|\exp(j2\pi r(x\cos\phi + y\sin\phi))dr\right]d\phi \qquad (7)$$

Equation 7 can be interpreted as a high-pass filtration of projection data, $S_\phi(r)$, using the filter function $|r|$. The filter is applied perpendicular to the projection direction and the frequency response is an ideal ramp filter. From equation 7, it can be seen that the integration should be carried out over all frequencies, but since the contribution of the Fourier coefficients above a certain frequency is negligible, the projections are considered to be band-limited. Because of this, the object can be sampled by observing the Nyquist criteria without introducing errors. By using a modified ramp filter instead of the ideal ramp filter ring artefacts in the reconstruction, caused by the sharp cut off of the filter, can be avoided. The ramp filter can be modified for instance by multiplying with a Hanning window, often used to smooth data when noise is present.

By back-projecting the filtered projections, an estimate of the object function *f(x,y)* is obtained.

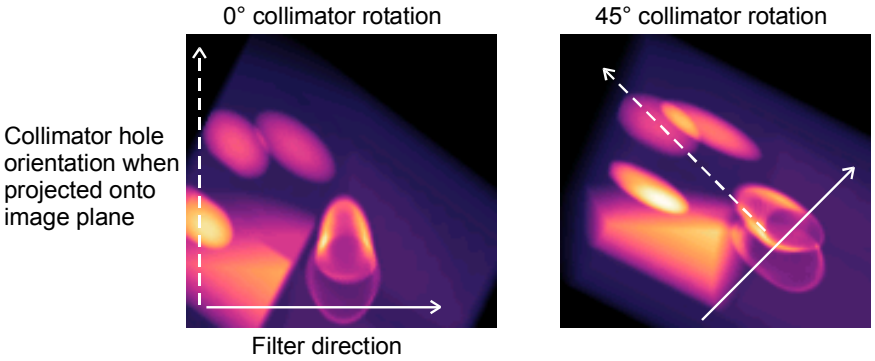

Figure 11. The reconstruction filter in Ectomography is applied tangentially to the projection direction. The dashed arrows indicate the collimator hole or projection direction when projected onto the image plane, while the solid arrows indicates the filter direction.

In Ectomography, the high pass filter is applied in a direction tangential to the angle of collimator rotation i.e. the direction of the projection, meaning that the filter direction is different in each projection image, as illustrated in figure 11. Section thickness is defined by applying a low-pass filter in a direction parallel to the direction of the projection. This is in contrast to SPECT, where filters are applied in the same direction for all projection images.

Iterative algorithms

Another approach to image reconstruction is to use statistical methods, such as the widely used Maximum Likelihood Expectation Maximization (ML-EM) [10]. In contrast to Fourier methods such as FPB, statistical methods do not explicitly attempt to invert the Radon transform. Instead, the process of image formation is considered, and in some way modelled in an iterative algorithm. Generally, the acquisition process is modelled as an over determined equation system, where we try to find the relationship between the projection data and the object function in an iterative manner, much as iteratively solving any equation system.

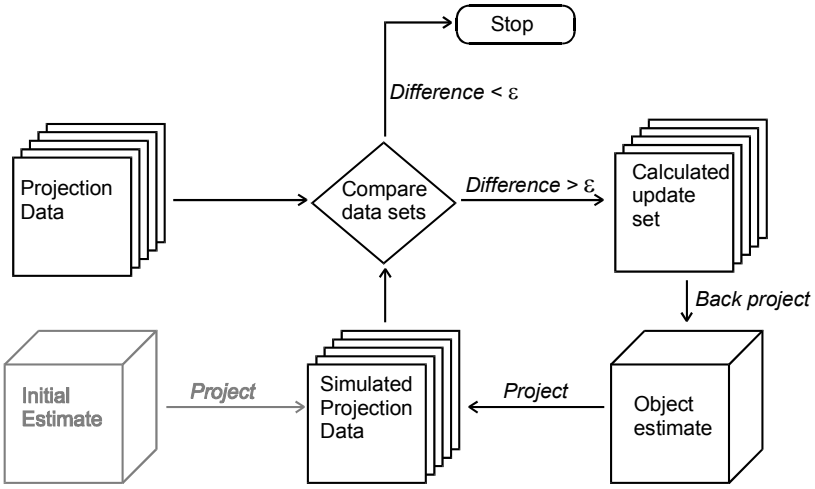

Figure 12. Schematic overview of an ML-EM

The ML-EM algorithm can be written as

$$f_i^{n+1} = \frac{f_i^n}{\sum_j c_{ij}} \sum_j \frac{c_{ij} p_j}{\sum_k c_{kj} f_k^n} \qquad (8)$$

where f is the object estimate, f_i represents the ith discrete element (pixel or voxel) in the object. The notation f^n denotes the object estimate after n iterations. The factor c_{ij} is the contribution of object element i to projection pixel j. The expression $\sum_k c_{kj} f_k^n$ can be interpreted as the forward projection of the nth iteration object estimate, resulting in a set of projection images.

If we define an update projection set u as

$$u_j = \frac{p_j}{\sum_k c_{kj} f_k^n} \qquad (9)$$

Observing equation 9, equation 8 can be written as

$$f_i^{n+1} = \frac{f_i^n}{\sum_j c_{ij}} \sum_j c_{ij} u_j \qquad (10)$$

The factor $\sum_j c_{ij} u_j$ in equation 9 is equivalent to a back projection of the update set u, essentially creating an update volume that is element-wise multiplied with the previous object estimate, and normalized using the factor $\sum_j c_{ij}$.

Implementation of Ectomography – The Cardiotom system

Mechanical construction

Rotating slant hole collimator

In order to make a mobile system, the total weight must be kept as low as possible. At the same time, the system must be mechanically balanced and stable. As a consequence, it is not feasible to move the detector head during data acquisition in order to obtain different projection directions. Instead of moving the entire detector head, the Cardiotom system uses a collimator with parallel, and slanted holes. To achieve different projection directions, the collimator is rotated in front of the scintillation crystal, as shown in figure 13. The rotation mechanism is integrated into the mounting of the collimator, and consists of an inner ring, onto which the collimator is attached, and an outer ring, which is mounted on the detector housing. The inner ring is mounted in a roller bearing on the outer ring .

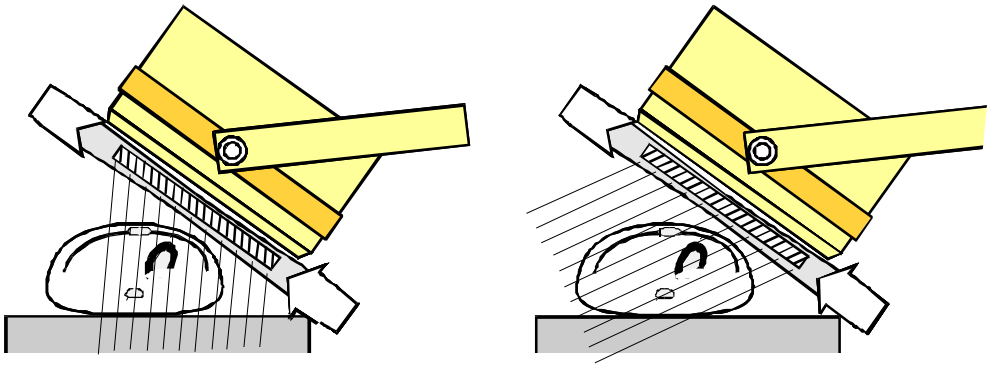

Figure 13. The rotating slant hole collimator and resulting view direction at 0° and 180° collimator rotation.

Segmented collimator

The Cardiotom system was primarily designed for myocardial imaging, and the heart is a relatively small organ. As a consequence, the projection of the myocardium on a detector with a diameter of 400 mm will occupy less than a quarter of the total detector area. Even for patients with myocardial disease and increased heart volume, the projection of the myocardium fits in a segment with a size of one quadrant. This makes it possible to use segmented collimators with up to 4 segments, where each segment has its own unique projection direction, but with the same slant angle. With this arrangement, the system sensitivity is increased by a factor approximately equal to the number of segments. The increase in system sensitivity can be utilized either to reduce radiation exposure, acquisition times, or to reduce noise by improving photon counting statistics. For seriously ill patients, the possibility of reducing acquisition times is most important. Today, collimators with one two, three and four segments have been designed and manufactured, with slant angles of 30°, 37.5° and 40°

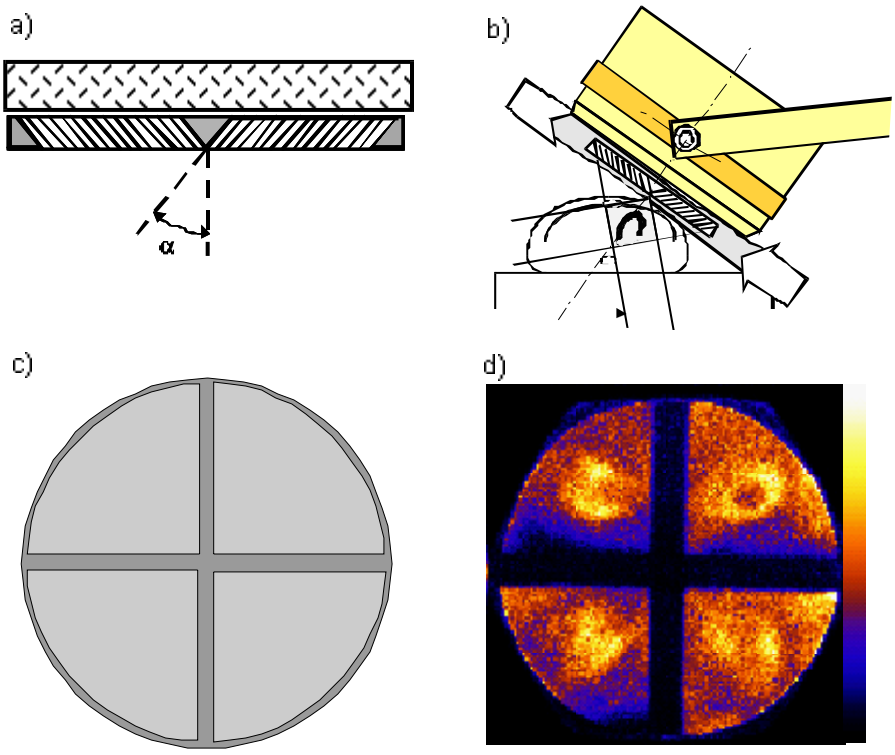

Figure 14. Illustration of a segmented collimator, and the acquisition geometry. a) is a cross-section of a 4 segment collimator, c) illustrates the segments and the dead zones between them. The system positioned for acquisition is shown in b) together with an example of a resulting projection image is shown in d).

Reconstruction volume

As indicated above, the reconstruction volume for data obtained with multi-segmented collimators has the shape of a double cone. This double cone is only symmetric for a 2-segment collimator, for all other cases it is to some extent asymmetric as illustrated in figure 15.

Consider a collimator with the following parameters

α:	slant angle
a:	thickness
n:	number of segments
D:	diameter of detector

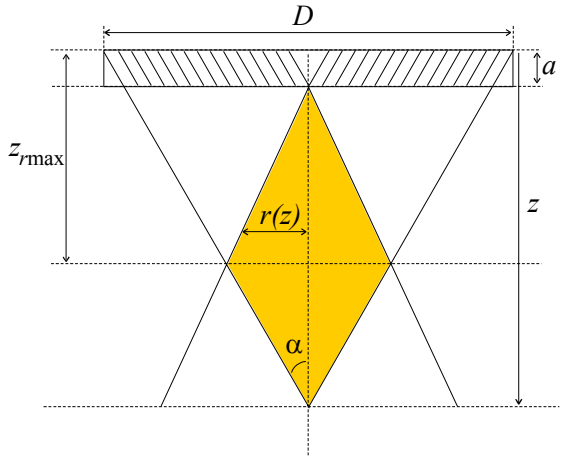

Figure 15. Common reconstruction volume for a collimator with two or more segment.

The thickness of septum between segments is then

$$l = a \tan\alpha \sin\left(\frac{\pi}{n}\right) \tag{11}$$

The distance from the detector at which the radius of the common reconstruction volume is largest is defined by:

$$z_{r\max} = \frac{\frac{D}{2} + l}{\tan\alpha\left(\sin\left(\frac{\pi}{n}\right) + 1\right)} \tag{12}$$

Equation 11 and 12 yields the radius of the common reconstruction volume, *r(z)*, which can then be expressed as Equation 13.

$$r(z) = \begin{cases} z\tan\alpha \sin\left(\frac{\pi}{n}\right) - l, & \text{for } z \le z_{r\max} \\ \frac{D}{2} - z\tan\alpha, & \text{for } z > z_{r\max} \end{cases} \tag{13}$$

Electronics and computer components

The Cardiotom system has been designed and built as a self-contained system for tomographic studies. The system comprises a detector head, Sopha DS7(Sopha Medical Vision), equipped with a rotating slant hole collimator, electronics for pulse discrimination and system control, and a computer (PC) for data processing and display.

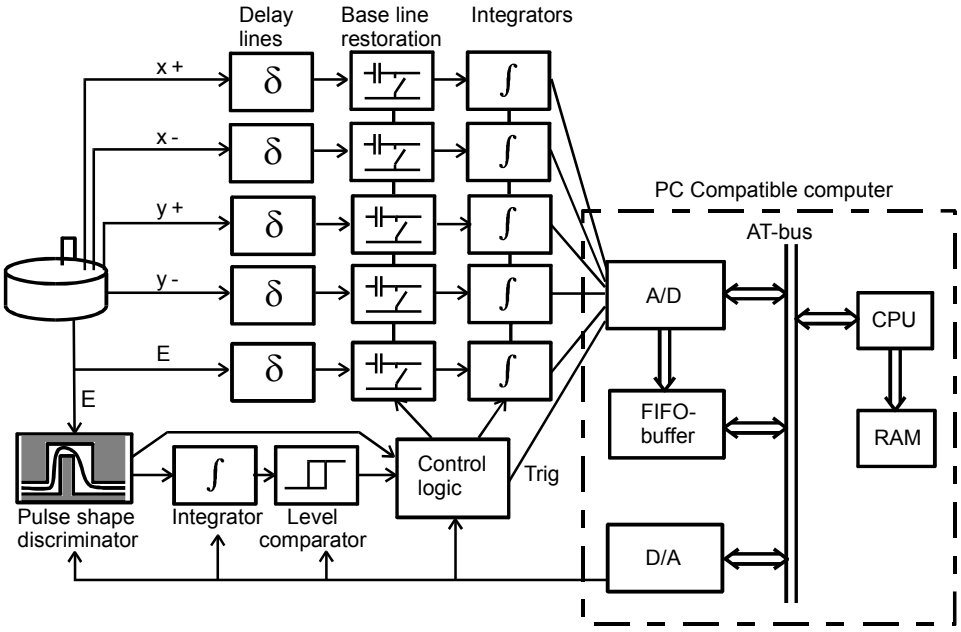

Figure 16. Block diagram of the data acquisition electronics.

The Anger detector delivers 5 signals (E, X+, X-, Y+, Y-) in the form of pulses with duration of about 1 μs. The E signal is used for determination of the event energy and the X+, X-, Y+ and Y- signals are used for determination of the event X Y-coordinates. The energy signal, E, from the detector is analysed by a pulse detector and shape analyser which also ensures that pulses are temporally well separated, figure 16. A coarse determination that the pulse is within the desired energy window is also performed at this point. If an event is accepted for further analysis, all five signals are integrated during 1.2 μs, starting 0.2 μs before the event. This is made possible through the use of delay lines in the signal path. The integrated E-signal is used to determine if the energy of the event is within the correct energy interval. When an event with the correct energy is registered, the control logic prepares for sampling of the integrated spatial signals. Here a pipeline structure is used in which the signals are held in sample-and-hold circuits until the AD-converter has completed conversion of the preceding event. All pulse height analysis parameters are set by reference voltages generated by a PC-based DA-board (ComputerBoards CIO-DA16). Further processing of the events is performed with software.

All signals from the detector head are digitised using a PC based AD-board (ComputerBoards CIO-AD16JR-AT). The maximum sampling frequency for 5 signals is 150 kHz, which translates into 30 000 events/second. The digitised values from the AD-board are stored in a separate First In First Out (FIFO) -buffer (ComputerBoards MEGAFIFO), which can hold up to 12.8 million events depending on the memory installed on the FIFO-buffer board. Currently, the memory installed allows 3.2 million events to be stored. The AD board uses a dedicated bus, called DT-connect, to communicate with the AD. This bus operates independently of the CPU and the ISA bus of the computer, which reduces the workload on the computer. Events are normally read sequentially from the FIFO buffer after each completed projection image, which allows the AD board to operate at full speed during acquisition of a projection.

The rationale for this design with its speed limitations is that at the outset of this project no data acquisition systems suitable for this kind of mobile applications were available. Today

several manufacturers have miniaturised designs utilising ASICs with excellent performance that can be used directly in our system.

Software

Software developed for the Cardiotom system can be divided into two categories. The acquisition software package handles data acquisition, initial reconstruction and presentation of section images, and the other software provides further image processing, such as reorientation, generation of polar maps, and iterative reconstruction algorithms.

The acquisition software controls the D/A, A/D and FIFO boards, so that the correct control voltages are applied to data acquisition electronics, setting the A/D voltage range and sampling modes of the A/D board and reading data from the FIFO board. To achieve the best possible count rate performance, the FIFO is not read during image acquisition, since the A/D has to be stopped in order to access data in the memory of the FIFO board.

Figure 17. Data flow during image acquisition.

The data flow of the acquisition software is shown in figure 17. The hardware FIFO buffer contains the raw sampled data in five channels, $x+$, $x-$, $y+$, $y-$ and E (energy). As the samples are read from the FIFO-buffer local energy discrimination is applied. Local energy discrimination is applied because the energy signal depends on detector position, i.e. an event registered at a position in the centre of a PM tube will yield a higher energy signal than an event registered at a position between two or three PM tubes because fewer light photons will be received at the photo cathode in the latter case. As only photons within a limited energy range are of interest, an energy window is defined. For ^{99m}Tc, the energy window is usually 140 keV ±10%. The local energy discriminator performs energy windowing based on the raw sample values, and incorporates the position dependence of the energy signal. To perform local energy discrimination, the system has to be calibrated. Calibration is performed by collecting local energy spectra from a ^{99m}Tc flood source– A local spectrum is collected for each pixel position, usually in a 64*64 matrix. From these energy spectra, an energy correction matrix is calculated, usually 64*64 elements, where each element contains a multiplicative offset factor relative to the mean spectrum, as measured over the whole detector field.

When a projection image has been collected, homogeneity correction is applied. The homogeneity correction compensates for position dependent sensitivity fluctuation after local energy discrimination. The planar image is element-wise multiplied with the homogeneity correction matrix, and added to the projection set. The homogeneity correction matrix is calculated from a flood field image, collected with the local energy discrimination applied.

When an acquired projection image is added to the projection set, it is filtered and back projected into the reconstruction volume. Therefore, section images of the reconstructed volume can be viewed almost immediately after the last projection image has been acquired.

The second software package includes further reconstruction algorithms, reorientation of reconstructed images and the construction of polar maps (bulls-eye plots). This package has been developed using an object-orientated paradigm using Borland C++ Builder. The

application allows several studies to be opened within the application i.e. for comparative measurements. Reconstruction algorithms have been developed as classes that operate on data, producing a reconstruction volume. Several algorithms have been implemented, such as filtered back-projection for Ectomography and filtered back-projection for SPECT, as well as iterative algorithms for both Ectomography and SPECT geometries.

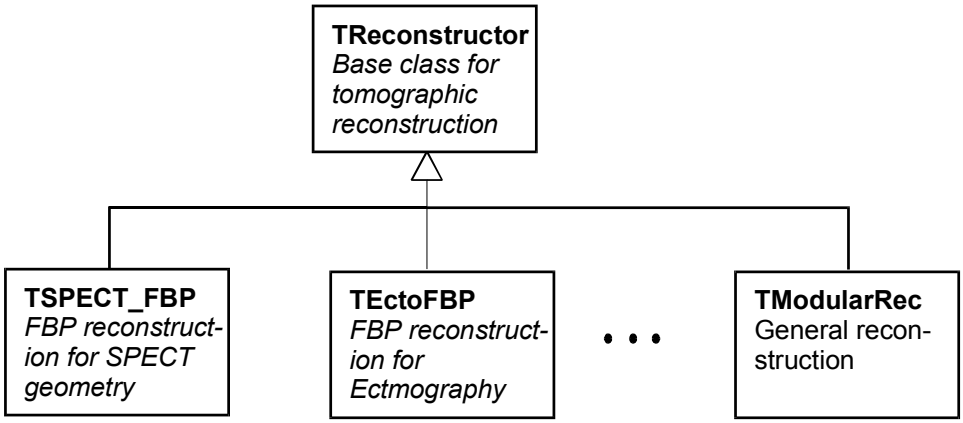

Figure 18. Class hierarchy for tomographic reconstruction.

While several specialized objects were initially implemented, they all inherit from a common class called *TReconstructor*. A more general class has also been implemented, called *TModularReconstructor*. As the name suggests, it takes a modular approach to tomographic reconstruction based on the fact that both iterative algorithms, such as ML-EM, and FBP can be described with a set of similar operators. In the current implementation, the modular reconstructor uses two or four operator, which are described by different classes. There are four base classes from which different acquisition geometries and algorithms may be implemented. It also has support for reconstruction using ordered subsets [11], a method used to speed up convergence in EM based algorithms (OS-EM).

The base operator classes are

- TBackprojector: describes and implements the back-projection process and geometry. It back-projects an update data set into a temporary target volume used later in the update/normalization step.
- TProjector: describes and implements the forward projection process and geometry in an iterative algorithm. It also creates a projection data set from the latest updated reconstruction volume.
- TDifferentiator: defines how the update data set is calculated based on measured data in relation to data from the TProjector class.
- TNormalizer: updates and normalizes the reconstruction volume based on the latest back-projection procedure. It also implements noise regularization in iterative algorithms.

The projector and back-projector classes together should describe the same acquisition geometry and currently Ectomography using rotating slant hole collimators and SPECT geometry have been implemented. For both geometries, there are variants in the class hierarchy for straight-line projection and depth dependent PSF projection. Normalisers currently implemented include ML-EM/OS-EM, TV-EM and TV3D-EM. The differentiators

include the update of projection data procedure for EM type algorithms, but may also be selected to be a filter if FBP reconstruction is to be performed.

In EM-type algorithms all four operators need to be initialised. As mentioned above, if the differentiator is a high-pass filter of correct orientation, it is also possible to perform FBP with TModularReconstructor. For FBP, only the back-projector, differentiator and normaliser should be initialised, and the number of iterations set to 1. A special copy normaliser that copies the temporary target volume to the reconstruction volume must also be used.

Verification

Misalignment & External activity

The Cardiotom system is primarily designed for acute studies. In an acute setting time is often limited, as is the physical space for manoeuvring the system. It is therefore, of importance to know how image quality is affected by the positioning of the camera. We have shown that using a 4-segment collimator with a slant angle of 37.5° or more, will allow for rapid positioning in myocardial imaging (II). The reduced volume due to collimator segmentation is still sufficient to accommodate the heart and artefacts caused by data truncation of activity external to the myocardium can be minimised or suppressed (IX).

Iterative reconstruction

Iterative reconstruction techniques have the advantage of being able to model the image formation process based on the underlying physics. Using iterative techniques it is, therefore, possible to incorporate factors such as attenuation, scatter and depth dependent collimator blurring into the reconstruction algorithm, and compensate for these factors. However, compared to Fourier methods and FBP, which are based on an analytical inversion of the Radon transform, iterative algorithms are generally much more computationally expensive. Bearing this in mind, the reconstruction algorithm chosen for Cardiotom system was the FBP, because it facilitated simultaneous image acquisition and reconstruction, yielding almost instant availability of reconstructed images on the completion of acquisition. However, an attempt to compensate for the distant depending collimator blurring in FBP reconstruction was shown to introduce distant depending noise patterns (VIII). With the steadily growing computational power, however, the basis for the choice of algorithm should probably be reviewed. Therefore, it is important to investigate what can be achieved with iterative reconstruction techniques.

A common class of iterative reconstruction algorithms are the ones derived from ML-EM algorithms. The ML-EM algorithm performs well on noise free data, but the presence of noise in projection images may cause ML-EM to increase the variance (or noise) in the reconstructed images with an increasing number of iterations [12].

We have investigated iterative EM-based algorithms and developed a 3D version of an algorithm based on the Total Variation (TV) Norm [13]. The Total Variation Norm was developed in the early 1990's by Rudin et al as a method for smoothing noise in 2D images, without causing excessive smoothing of edges present in the images. The TV-norm was extended to 3D and used as a prior in Green's algorithm [14]. It has yielded promising results, both in improving depth resolution and reducing noise in reconstructed images form limited view angle tomography (IV). An example using a voxelised cardiac phantom (figure 19), illustrates how image quality improves using TV3D-EM, shown in figure 20.

The improvement in depth resolution is also evident when looking at the Fourier representation of a small point with Gaussian intensity distribution, reconstructed using FBP and TV3D-EM. Figure 21 illustrates this, by showing a slice through the origin of the Fourier domain, oriented parallel to the z-axis (or depth direction), as shown in figure X. Notice how the empty cone is at almost perfect agreement with what the Fourier slice theorem predicts, while it is very much diminished when reconstructed using TV3D-EM .

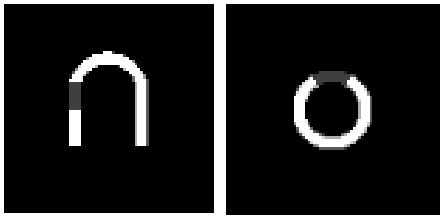

Figure 19. Voxelised cardiac phantom Long axis section (left) and short axis section (right).

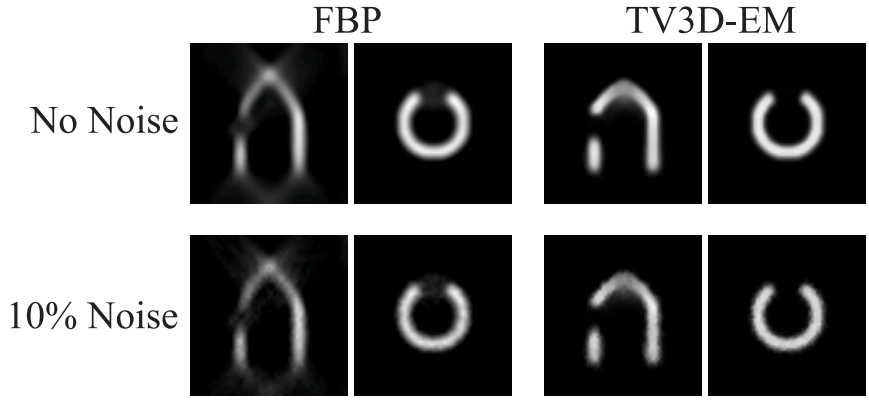

Figure 20. Long axis and short axis images reconstructed from noise free and noisy data sets, simulated from a voxelised cardiac phantom

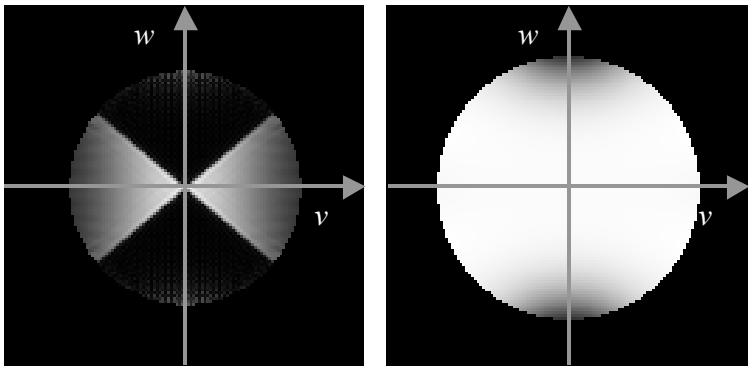

Figure 21. The frequency response of a reconstructed object consisting of a small point with a Gaussian intensity distribution in space. The images are a cross section through Fourier space illustrating the empty cone in FBP reconstruction (left) and how this cone in some sense is filled when the same object is reconstructed with TV3D-EM.

The 2D TV-norm has been tested in the reconstruction of transmission images from SPECT by Panin et al [*15*], and yielded promising results. However, since SPECT imaging and reconstruction uses 2D projection data to reconstruct 3D volumes, it was considered of interest to compare the 2D TV-norm to the 3D TV-norm. Hence, the 3D algorithm developed for Ectomography was also implemented and evaluated for SPECT geometry (V). It was shown to lead to an improvement in image quality when compared to the 2D TV-norm, mainly due to better conditioning of noise.

Discussion

Currently, three prototype systems have been designed and built. The first system, Cardiotom Mark 1, was designed and built in 1993. The initial system comprised a General Electric MaxiCamera interfaced with a PDP-11 (Digital Equipment Corp.) computer using the GE detector electronics. The system actually consisted of two units, the camera unit and the computer rack. The camera unit was built on an industrial forklift truck, with motorized camera detector elevation. In a modification of Cardiotom Mark 1, a computer (PC), equipped with a data acquisition card form ComputerBoards replaced the PDP-11. While the total weight of the system was 655 kg, the mobility improved substantially with this redesign. Despite the weight and size of the Cardiotom Mark 1, it was used in more than 200 patient studies, some of them in the intensive care unit. The patients in intensive care included a group studied within one-hour post coronary bypass surgery [16]

A second system named Cardiotom Mark 2 has been designed and built(VI). This system has improved mobility and is based on a commercial gamma camera detector (Sopha DS-7), for which housing has been designed with lead shielding optimised for myocardial imaging with ^{99m}Tc. The detector is mechanically counter-balanced to provide weightless movement. Detector electronics have been designed to interface the detector with the data acquisition board in the computer and also to provide pulse height discrimination. As a result of the modifications, the weight has been reduced to 350 kg. Among other things, this system was used to perform an animal study regarding early reperfusion of the myocardium and final infarct size (III). A third prototype, (Cardiotom Mark 3) very similar to Mark 2, has also been built. It is somewhat lighter at 320 kg, and a few centimetres narrower than its predecessor in order to improve manoeuvrability.

All three systems have been used clinically. So far, the majority of the studies performed have been cardiac studies, both human and animal studies. More than 100 phantom studies, focused mainly on heart phantoms, have been performed with these systems in order to investigate the Ectomographic technique. A comparative study with SPECT as reference has shown that the diagnostic information obtained with the Cardiotom system is equivalent to that obtained from SPECT, when data are viewed as short axis slices and polar maps [17].

Pilot studies concerning brain imaging have also been performed, and the results of these warrant further investigation (VII). The quality obtained from these studies indicates a need to reduce artefacts arising from the limited depth resolution caused by the empty cone. One possibility is to use iterative techniques such as TV3D-EM or COMET [18] since these reconstruction techniques utilize the information available in the projection data more effectively. Preliminary results using TV3D-EM indicate that artefacts arising from the limited depth resolution are greatly reduced, as seen in figures 19,20 and 21. The TV3D-EM has been implemented on the Cardiotom platform.

Another issue regarding the choice of reconstruction algorithm is the computational complexity. For studies of an acute nature, where images are required immediately after completed acquisition, filtered back-projection is currently the only option. With the present implementation of the iterative algorithms, image reconstruction requires between 20 – 40 minutes when performed on a computer equipped with a single Intel Pentium III/600MHz processor, depending on the number of subsets and iterations chosen. There are, however, several ways of improving the reconstruction time of a given algorithm. Perhaps the most obvious would be to use a faster CPU, combined with motherboard and memory circuits for faster memory access. A second alternative would be to use multiple processors, and rewrite the reconstruction algorithms to allow parallel execution of several projector/back-projector

pairs. Given the current implementation this should not require major modification. A third alternative is to rewrite part of the code to improve the speed, using SIMD (Single Instruction/Multiple Data) instructions available in Pentium III and newer Intel processors. Obviously, a combination of all three methods would provide the greatest efficiency.

An alternative approach that is currently being used, is to do an initial reconstruction using FBP, obtaining images bedside, then performing a second reconstruction with an iterative algorithm to obtain images of higher quality for more detailed analysis.

Conclusions

- Software has been developed for the acquisition and presentation of Ectomographic data and implemented on a mobile tomographic gamma camera system: Cardiotom. Three systems have been developed and for clinical studies.
- The limitations of Ectomographic acquisition when using filtered back projection for data reconstruction have been studied. It has been shown that it is possible to effectively suppress artifacts arising from data truncation in simulated data when using segmented collimators in Ectomography. Problems due to the limited depth resolution are inherent to the method of reconstruction.
- A three-dimensional iterative reconstruction technique TV3D-EM has been developed for use with Ectomography. The algorithm has also been adapted for the reconstruction of SPECT data.
- The Cardiotom system has been shown to be viable for use in a clinical situation

Acknowledgements

I wish to express my sincere gratitude and appreciation to all those involved in this project and making this thesis possible. In particular I would like to thank:

Susanne Dale-Ekdahl for introducing me into the world of mobile tomographic gamma cameras, for her inspiration and support.

Dianna Bone, for continuous support, advice and clinical knowledge. Always encouraging, with kind humour and for thoroughly reviewing this thesis and much of the material therein.

Professor Håkan Elmqvist for his great ideas and broad competence, making the project possible.

All the staff at the Department of Medical Engineering for their friendship and support.

My wife, Katja, without whose moral and emotional support finally made this thesis happen.

My parents, for always believing in me.

The National Board for Technical Development who financially supported parts of this project.

References

1 Anger H O. Scintillation camera. Rev Sci Instrum 1958;29;27-33

2 Hilton TC, Thompson RC, Williams HJ, Saylors R, Fulmer H, Stowers SA. Technetium-99m sestamibi myocardial perfusion imaging in the emergency room evaluation of chest pain. J Am Coll Cardiol 1994 23:1016-22

3 Wackers FJTh, Heller GV, Stowers S, Hendel RC, Herman S, Baron J, Daher E. Prognostic value of normal rest tetrofosmin SPECT in patients with acute chest pain and nondiagnostic ECG in emergency department. J Nucl Card 1997; 4: S26

4 Radensky PW, Hilton TC, Fulmer H, McLaughlin BA, Stowers SA. Potential cost effectiveness of initial myocardial perfusion imaging for assessment of emergency department patients with chest pain. Am J Cardiol 1997; 79: 595-599.

5 Edholm P, Granlund G, Knutsson H, Peterson C. Ectomopraphy. A new radiographic method for reproducing a selected slice of varying thickness. Acta Radiol 1980;21:433-442.

6 Hilton TC, Thompson RC, Williams HJ, Saylors R, Fulmer H, Stowers SA. Technetium-99m sestamibi myocardial perfusion imaging in the emergency room evaluation of chest pain. J Am Coll Cardiol 1994 23:1016-22

7 Wackers FJTh, Heller GV, Stowers S, Hendel RC, Herman S, Baron J, Daher E. Prognostic value of normal rest tetrofosmin SPECT in patients with acute chest pain and nondiagnostic ECG in emergency department. J Nucl Card 1997; 4: S26

8 Radensky PW, Hilton TC, Fulmer H, McLaughlin BA, Stowers SA. Potential cost effectiveness of initial myocardial perfusion imaging for assessment of emergency department patients with chest pain. Am J Cardiol 1997; 79: 595-599.

9 Radon J. Über die bestimmung von Funktionen durch ihre Integralwerte längs gewisser Mannigfaltigkeiten. Berichte Sächisische Akademie der Wissenshaften, Math.-Phys Kl.,69 262-267 Leipzig 1917

10 Shepp L A, Vardi Y. Maximum Likelihood Reconstruction for Emission Tomography. IEEE Trans Med Imaging. 1982;MI-1:2;113-122.

11 Hudson H M, Larkin R S. Accelerated image reconstruction using ordered subsets of projection data. IEEE Trans. Med. Imaging. 1994;13;601-609.

12 Lalush D S, Tsui B M W. Simulation evaluation of Gibbs prior distributions for use in maximum a posteriori SPECT reconstructions. IEEE Trans. Med. Imaging. 1992; 2 :267-275

13 Rudin L I,Osher S, Fatemi E. Nonlinear total variation based noise removal algorithms. Physica D 1992:**60;** 259-268.

14 Green P J. Bayesian reconstructions from emission tomography data using a modified EM algorithm. IEEE Med. Imaging 1990:9; 84-93

15 Panin V Y, Zeng G L, Gullberg G T. Total variation regulated EM Algorithm. IEEE Trans. Nucl. Sci. 1999; (46)6**:** 2202-2210.

16 Anderson RE, Bone D, Dale SM, Lindström C, Öwall A, Brodin L-Å. Myocardial perfusion after coronary artery bypass graft surgery: A study using ectomographic myocardial scintigraphy study and adenosine provocation. Scandinavian Cardiovascular Journal. 32(2):69-74, 1998.

17 Dale S, Bone D, Brodin L-Å, Lindström C. Comparison of SPECT and Ectomography for evaluating myocardial perfusion with technetium-99m-sestamibi. J Nucl Med 1997; 38:754-759.

18 U Skoglund, Öfverstett L-G, R Burnett, G Bricogne. Maximum entropy three dimensional reconstruction with deconvolution of the contrast transfer function: a test appliction with adenovirus. J Struct Biol 1996; 116:173-188.